

Searching anomalies using nonlinear dimensionality reduction techniques

X. Yang^{1,2,3*}, G. Hobbs³, S.-B. Zhang^{1,3}, A. Zic³, L. Toomey³, Y. Li², J.-S. Wang⁴,
S. Dai³, X.-F. Wu^{1,2}

¹ Purple Mountain Observatory, Chinese Academy of Sciences, Nanjing 210023, China

² School of Astronomy and Space Sciences, University of Science and Technology of China, Hefei 230026, China

³ CSIRO Space and Astronomy, Australia Telescope National Facility, PO Box 76, Epping, NSW 1710, Australia

⁴ Max Planck Institute for Plasma Physics, Boltzmannstraße 2, D-85748 Garching, Germany

28 June 2024

ABSTRACT

We have searched for anomalous events using 2,520 hours of archival observations from Murriyang, CSIRO’s Parkes radio telescope. These observations were originally undertaken to search for pulsars. We used a machine-learning algorithm based on ResNet and Uniform Manifold Approximation and Projection (UMAP) in order to identify parts of the data stream that potentially contain anomalous signals. Many of these anomalous events are radio frequency interference, which were subsequently filtered using multibeam information. We detected 202 anomalous events and provide their positions and event times. One of the events could potentially come from a white dwarf. Some of them may originate from stellar flares, lightning, or be true anomalies, which are currently of an unknown type.

Key words: fast radio bursts; transients, methods: data analysis; astronomical instrumentation, methods, and techniques

1 INTRODUCTION

Radio astronomy is a subject full of surprises. From 1933 to 1997, 17 key discoveries in radio astronomy were found (Wilkinson et al. 2004). These discoveries can be divided into two classes, seven were made by testing a theory prediction (these were the “known-unknowns”), and ten were unexpected results found by chance (the “unknown-unknowns”) (Norris 2017). One unexpected highlight in the 21st century was the discovery of Fast Radio Bursts (FRBs). FRBs are bright radio pulses with a short duration (typically milliseconds) and the first FRB was discovered in archival data from CSIRO’s Murriyang Parkes 64 m-diameter radio telescope (Lorimer et al. 2007). It took six more years before Thornton et al. (2013) found four more FRBs. The large implied distances and the extremely high energies of FRBs mean they are intrinsically interesting and can be used for cosmological studies. As FRBs can now be considered as “known-unknown” sources, the Canadian Hydrogen Intensity Mapping Experiment (CHIME), the Australian SKA Pathfinder (ASKAP) and many other telescopes explicitly design their pipelines in order to find more FRBs and the number of known sources is rapidly increasing.

Most of the survey-related software in radio astronomy has been designed for searching for signals with specific characteristics. For example, PRESTO¹ (Ransom 2011) can search for pulsar and FRB signals which are characterised with a dispersion measure and pulse width and, for pulsar searching, the pulsation period. HEIMDALL²

has been explicitly designed to search for FRBs following the dispersion measure law. As quantified by Yong et al. (2022), these software packages become less effective as the signal deviates further from the expected properties.

We know that our data sets likely contain currently undetected “unknown-unknown” sources. For instance, ultra-long-period radio sources have been detected with Murchison Widefield Array (Hurley-Walker et al. 2022), a complete understanding of the radio emission from flaring stars on various time scales is still not perfectly understood and major surveys are being carried out with radio telescopes in order to search for technosignatures (Sheikh et al. 2021a; Ma et al. 2023).

One approach for finding the “unknown-unknowns” is machine learning. Webb et al. (2020) used HDBSCAN and t-SNE as anomaly detection algorithms and found seven uncatalogued variables and two stellar flare events. Giles & Walkowicz (2019) utilized the t-SNE algorithm to identify <4% of each season’s data as outlying in the Kepler field data. Gupta et al. (2022) trained a self-organizing map (SOM) to select 0.5% of the most complex and peculiar sources from ASKAP data. Marianer et al. (2021) combined a deep residual network (ResNet) and UMAP to search for spectrograms with anomalous patterns in public LIGO data.

Our research focuses on the Parkes archive pulsar search mode data (Hobbs et al. 2011). Zhang et al. (2020) found five previously undetected Rotating radio transients (RRATs) and one FRB in the Parkes archive dataset from 1997 to 2001. Zhang et al. (2019) found an FRB in the same dataset as the Lorimer burst, a remarkable twelve years after the discovery of the latter. We believe there are still plenty of gems to be collected in this archive.

Previous machine learning algorithms that have been developed to search for anomalies follow a procedure similar to the following:

* E-mail: yangxuan@pmo.ac.cn, (XY); George.Hobbs@csiro.au, (GH); sbzhang@pmo.ac.cn, (SBZ); xfwu@pmo.ac.cn, (XFW)

¹ <https://www.cv.nrao.edu/~sransom/presto/>

² <https://sourceforge.net/projects/heimdall-astro/>

- (1) They first extract features from the raw astronomical data.
- (2) Dimensionality reduction for high-dimensional data is carried out to enable the resulting data to be visualised.
- (3) The low-dimensional data are clustered, and anomaly ranking or outlier detection methods are applied.

Dimensionality reduction techniques play an important role in visualizing high-dimensional data. One widely used method is Principal Component Analysis (PCA), a well-established linear technique. PCA involves combining the original variables to derive principal components, enabling a reduction in the dimensionality of the data (Abdi & Williams 2010). Nevertheless, nonlinear techniques continue to grow in popularity and are better suited for effectively addressing the issue of overcrowding in data feature extraction. Prior to 2018, the t-Distributed Stochastic neighbour Embedding (t-SNE) was the most popular nonlinear technique in single-cell analysis (Van der Maaten & Hinton 2008). However, UMAP has since become more favoured among scientists due to its swiftness and ability to retain both local and global data structures (McInnes et al. 2018).

In our paper, we implemented ResNet, UMAP, and spectral clustering to accomplish the three stages. This pipeline was applied to datasets from the Parkes archive to search for any possible outlier. The time-frequency images derived from the raw data were used. In Section 2, we provide a description of the data and algorithms used in this study. The results of our clustering analysis are presented in Section 3, while Section 4 includes a discussion of our findings.

2 IMPLEMENTATION

The data used in this study was obtained from the Parkes archival data P269, a deep survey of the Large and Small Magellanic Clouds (Crawford et al. 2001; Manchester et al. 2006). This particular dataset was chosen as a representative sample of archival data containing anomaly events. It encompasses the initial discovery of FRB (Lorimer et al. 2007), and another weaker FRB was detected from this dataset twelve years later (Zhang et al. 2019). The sample time, spectra per subintegration, central frequency, bandwidth, and number of channels for these observations were 1000 μ s, 4096, 1374 MHz, 288 MHz, and 96, respectively. We processed all of the data in P269-2001JANT, which contains 2,258 files and 2,520 hours of integration time.

We also converted some artificial signals into time-frequency pixels, and injected them into the real observation data using the software described in Luo et al. (2022). The artificial signals were downloaded from the Cosmic Call 2003 message (Dumas 2007). As shown in Fig. 1, the 22 Cosmic Call images were resized into four distinct sizes, and subsequently distributed across a range of dispersion measure (DM) values, spanning from 0 to 4,000 with a step size of 800. This batch of simulation data is later used as a tracer in order to help locate the possible anomalies in the real data.

In brief, for our processing:

- (i) We selected the PSRFITS input files in groups of three. For each group, we also added in the Cosmic Call data file that will be used as a tracer for anomalous events.
- (ii) Each of these four data files was first read by the python package `ASTROPY`. Almost all files contained 2,051 subintegrations (shorter files are calibration observations and files which ended early). Each subintegration containing 96×4096 points was indexed and output as a 256×256 image. The image refers to 4.096 seconds of observation. We therefore obtain 2,051 images for each of the four data files.

(iii) We then employed a pre-trained ResNet50V2 model to extract features from each image and obtained a 512D feature vector that represents a compressed version of the original image.

(iv) The 512D feature vectors were then input to UMAP. This gives us a UMAP embedding for all the images in the four input files. Similar-looking images will appear close to each other in this UMAP embedding.

(v) We searched for different clusters in this UMAP embedding using “spectral clustering” and silhouette coefficient values.

(vi) We now have identified the different clusters corresponding to the images produced from the four input files. The clusters that contain more than 50% of Cosmic Call points are classified as clusters that potentially contain anomalous signals of interest.

(vii) For each cluster containing anomalous signals we record the corresponding input file properties and the time of the event.

This process is then repeated until all the input 2258 files are processed, and we have a large catalogue of potentially anomalous signals in the time-frequency domain. In order to identify signals worth further investigation we then repeat the UMAP process using all the images identified as potentially containing an anomaly. These then also get clustered and we finally inspect examples of each cluster by eye.

In more detail, for part (iii), we restructured the ResNet as illustrated in Fig. 2. We eliminated the final two layers and added an adaptive max pooling layer, along with two fully connected layers containing 512 and 128 neurons, respectively, activated by rectified linear units (ReLU). The model used parameters identical to those in our previous work for a similar task of extracting features from astronomical data (Yang et al. 2023).

For part (iv), we made use of a UMAP algorithm implemented in Python³. To optimize the clustering results, we tuned two UMAP parameters: `N_NEIGHBOURS`, `MIN_DIST` and one hyper parameter `N_SAMPLES`. `N_NEIGHBOURS` represents the size of the local neighbourhood and affects the balance between local and global structure in the data. Larger values of `N_NEIGHBOURS` will make the UMAP focus on a broader structure of the data, but may lose more detailed information. `MIN_DIST` controls the minimum distance between points in the low dimension and helps to preserve the broad topological structure. `N_SAMPLES` means how many samples we feed into UMAP each time. The chosen values for the number of samples in each batch affect the result. Too small `N_SAMPLES` may cause underfitting and lower the computation efficiency. Too large `N_SAMPLES` may exceed the computation memory or cover up the outlier signals. We performed a grid search for these parameters, `N_NEIGHBOURS` range from 2 to 1000, `MIN_DIST` range from 0.01 to 0.99, `N_SAMPLES` range from 500 to 50,000. Finally `N_NEIGHBOURS=10`, `MIN_DIST=0.01` and `N_SAMPLES=6,000` are determined for the P269-2001JANT dataset.

In part (v), instead of identifying regions by eye, we made use of “spectral clustering”, which is a widely adopted algorithm to identify specific clusters of data points. This normally gives better results compared to traditional approaches such as k-means. The methodology behind spectral clustering lies in utilizing the eigenvectors of a similarity matrix to effectively partition the data into clusters. In this algorithm, the data points assume the role of nodes within a graph. It transforms the clustering task into a graph partitioning problem. In order to estimate the clustering results, a grid search was conducted, exploring a range of cluster numbers from 2 to 10. Throughout this search, the effectiveness of the clustering was evaluated by considering the silhouette coefficient values. The silhouette coefficient serves

³ umap-learn.readthedocs.io

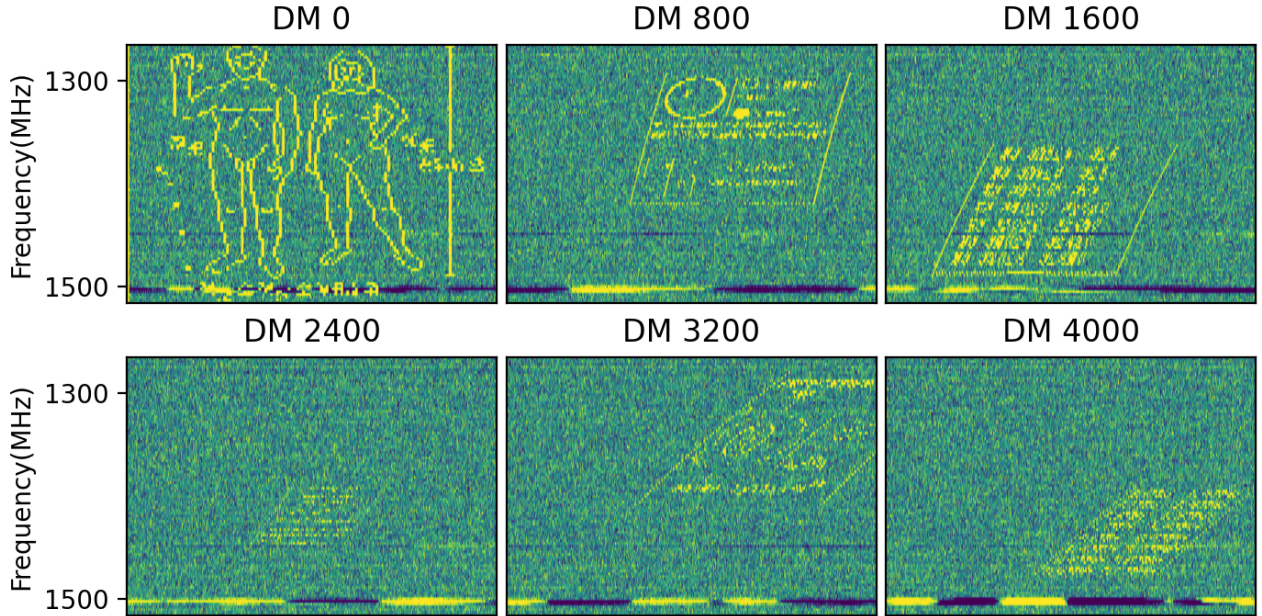


Figure 1. Six samples of the injected Cosmic Call data. Each figure refers to 4.096 seconds of integration time. The title of each figure shows the DM of the injected Cosmic Call data.

as a metric to assess the degree of cluster coherence, ranging from -1 to 1 . Values closer to 1 indicate well-defined clusters, while a coefficient greater than 0 indicates a satisfactory outcome.

The processing steps described above were implemented using multiple python scripts on the high-performance computer (HPC) infrastructure provided by CSIRO.

3 RESULTS AND DISCUSSION

3.1 Rediscovery of the Lorimer burst

In order to test our algorithm, we selected the data file containing the Lorimer burst along with data files corresponding to other beams in the same observation. We then processed these data in the same manner as described above. Our UMAP result is shown in Fig. 3. The input images containing the Cosmic Call signals are shown as a green cross. These generally cluster in the top-right region of the Figure. As the injected Cosmic Call signals become weaker then they form clusters that are slightly harder to distinguish from the normal data. Very roughly, the Figure divides into a few regions. On the left, the majority of the images contain no apparent signal, but can contain some persistent RFI. The bottom right region by eye looks very similar and no clear anomalous signals are seen. The strongest signals are in the upper right part of the Figure. We note that the second FRB discovered in this data set (Zhang et al. 2019) is undetectable by eye in the raw data stream and clusters with the “Normal data” in these UMAP results.

With the help of the tracer method and spectral clustering algorithm, the embedding data points are separated into eight clusters shown in Fig. 4 left-hand panel. The clusters which contain more than 50% of Cosmic Call points are classified as anomaly clusters (AN1 and AN2), other clusters are indicated as ND1 to ND6 where ND stands for non-detection of anomalous signals. Considering the total image quantity, this leads to a reasonable true positive and false

positive rate. Table. 1 shows the number of candidates, how many Cosmic Call signals are within the cluster, and how many images are classified as being not an anomaly (non-detection). The data points in AN1 and AN2 were classified as anomaly candidates and further checked by eye. The Lorimer burst is easily detected in AN1. The AN1 cluster also contains some strong RFI. The AN2 contains some weaker signals which are confirmed as narrowband RFI.

In the right-hand panel of Fig. 4, the silhouette coefficient values of the clusters are presented. The red dotted line represents the average silhouette coefficient, which exceeds 0.4 . This successful re-detection of the Lorimer burst provides confidence that our UMAP pipeline has the ability to find signals of potential interest. We therefore applied the pipeline to the entire P269-2001JANT data set.

3.2 Anomalies in the data set

After processing our entire data set, 27,308 images were identified as containing potential anomalies from the 2,320,167 raw data images. We need to distinguish astronomical sources from terrestrial sources of interference. With a single-dish radio telescope, this is non-trivial (Sheikh et al. 2021b). However, the use of the multibeam receiver allows some ability to distinguish ground-based signals from astronomical signals. In particular, any weak astronomical signal would only be seen in a single beam. For very strong signals (such as the Lorimer burst) we would expect to detect the same signal in a few adjacent beams. Any signal seen in a large number of beams or in widely separated beams can therefore be considered to be interference. We automatically searched for candidates seen simultaneously from more than three beams and rejected these as being caused by RFI. After this filter, the number of images decreased to 10,451.

Finally, a visual inspection was conducted on all of these images. The UMAP process did often miss weak events in some beams and therefore we carried out a visual inspection on these remaining candidates. We found that the majority were weak events in all 13 beams

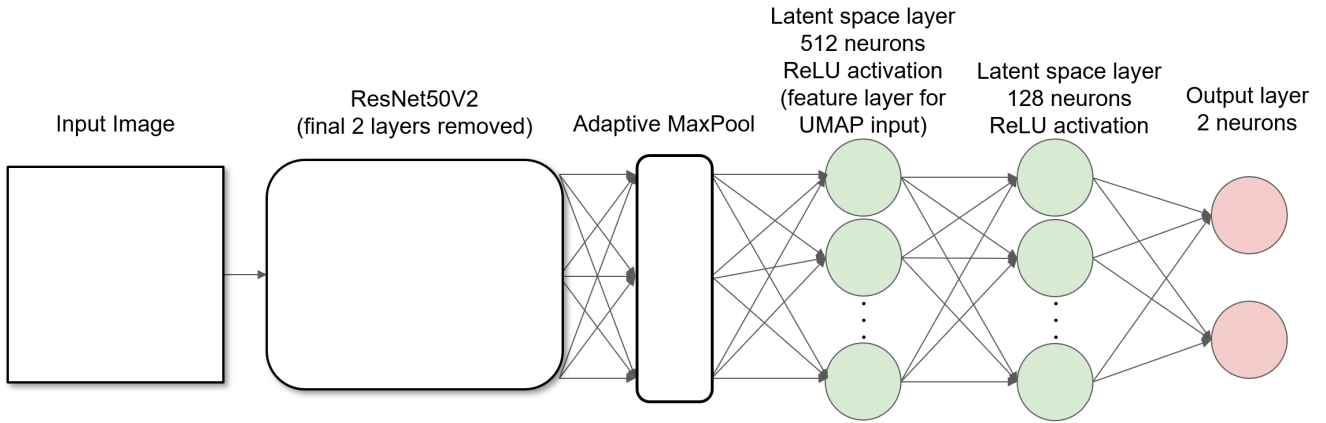


Figure 2. The input 256×256 image serves as the initial input to the pre-trained ResNet50V2 model. The last two layers of the pre-trained network have been replaced with an adaptive max pooling layer. This is then followed by two fully connected layers, consisting of 512 and 128 neurons, respectively. Activation of these layers is achieved through the ReLU activation function. In this work, the output layer utilized is actually the 512 neuron layer.

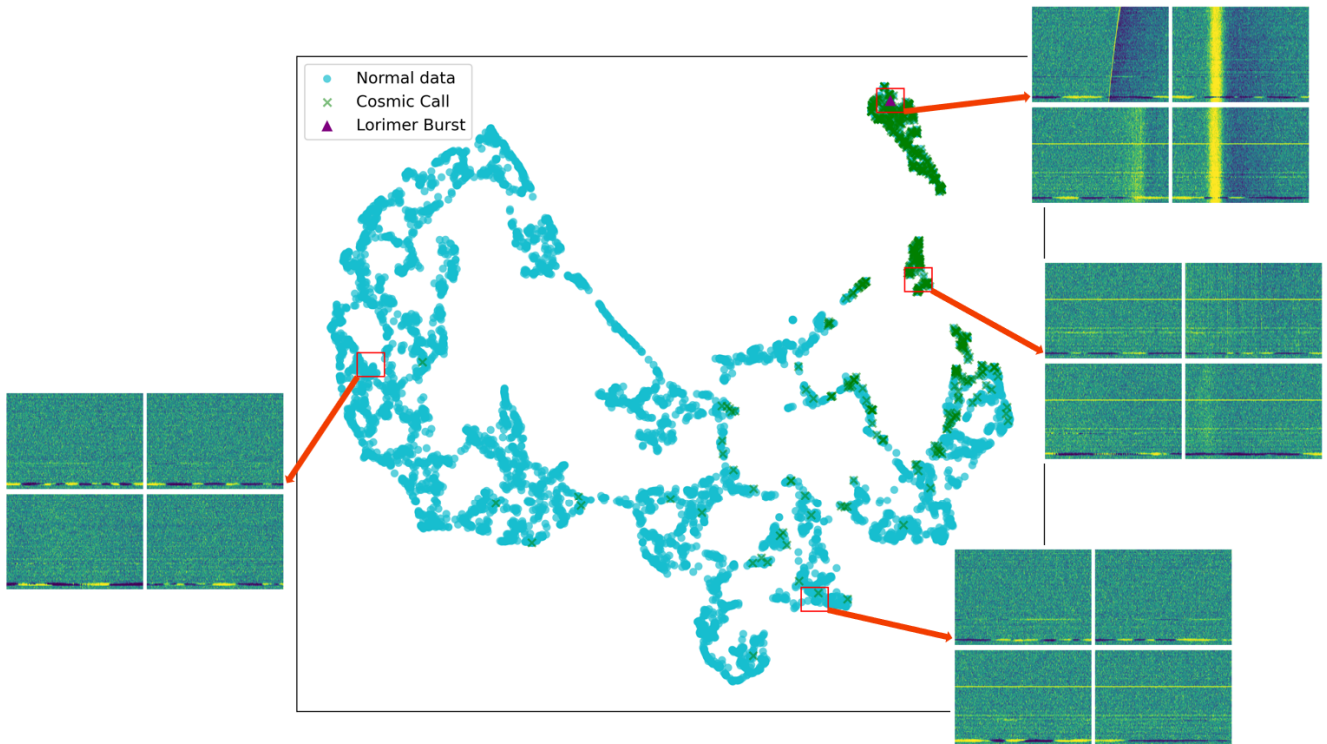


Figure 3. The UMAP embedding of 3 data files and cosmic call images. The pink triangle represents the Lorimer burst, and each cyan dot represents an image containing 4.096 seconds of observation. The four red squares show some representative images of the adjacent areas.

and hence rejected these manually, leaving us with 202 potential events. Most of these were detected in only one beam of the multi-beam system. In no case have we observed signals that appear in multiple beams but not in adjacent ones. Table 3 lists the properties of these anomalies.

In order to search for commonalities between these 202 events, we show the UMAP embedding of these anomalous events in the left-hand panel of Fig. 5. The embedding was also divided into eight clusters using spectral clustering and marked with different colours. The right-hand panel of Fig. 5 shows two representative figures of each cluster. We can find some morphological similarities inside each cluster. For example, cluster one contains images with

bright signals where the digitizer saturated during the event and took time to recover, which includes the Lorimer burst. The images in cluster six are dominated by saturation effects occurring after bright events, although these events only happened in one beam of the multi-beam system. In most cases, this is likely to be a strong RFI signal in the pointing direction of that particular beam (the beam patterns for a source in the sky are described by Ravi et al. (2016)), but these sources are worth follow-up study and we discuss one such event below. The images corresponding to cluster eight show broadband signals each lasting around a second, but only detected in a single beam. On this scale, we see no evidence of any dispersion in these signals. Signals with these characteristics occur several times

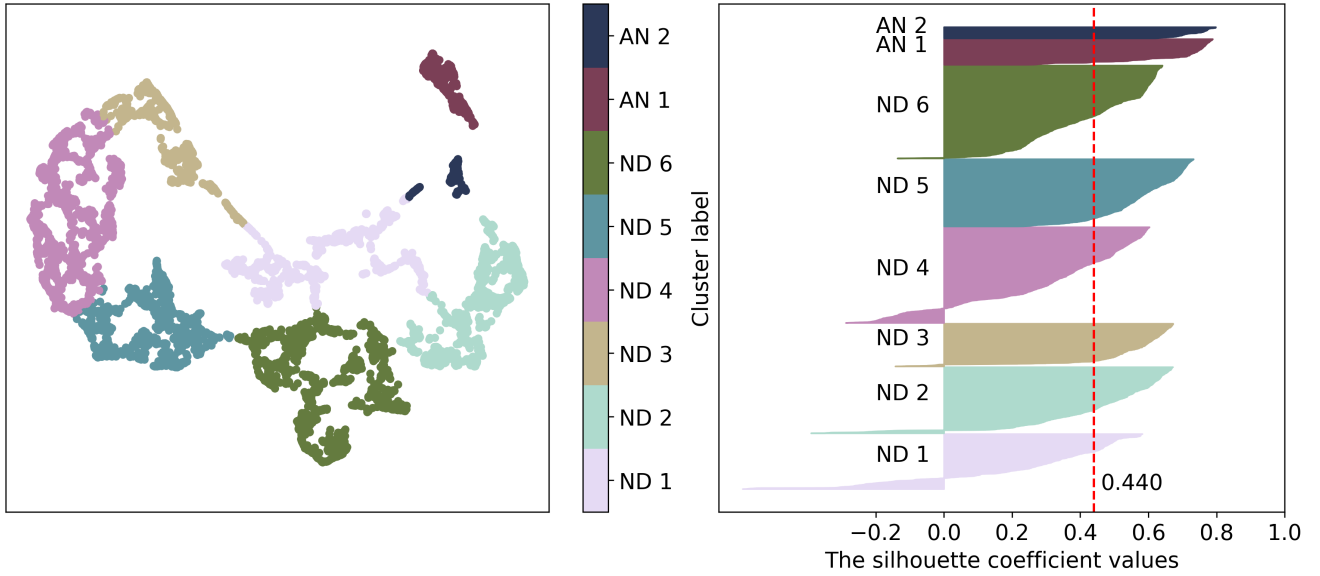


Figure 4. The left panel is the spectral clustering result of UMAP embedding in Fig 3. The label ND means non-detection cluster and AN means anomaly cluster. The right-hand panel corresponds to silhouette coefficient values. The red dotted line in the right panel represents the average silhouette coefficient value of the clusters.

Table 1. The information of the spectral clustering result of UMAP embedding. There are two anomaly clusters, the data points in anomaly clusters are classified as anomaly candidates.

	Total number	Cosmic Call number	Anomaly candidate number	Non-detection number
Non-detection 1	826	43	0	783
Non-detection 2	992	125	0	867
Non-detection 3	641	0	0	641
Non-detection 4	1436	1	0	1435
Non-detection 5	1009	4	0	1005
Non-detection 6	1393	18	0	1375
Anomaly 1	386	366	20	0
Anomaly 2	169	142	27	0

at various positions in the sky throughout a relatively short data span (the data span is from March to June in 2001) and persist for a few seconds on each occurrence. These events do not always occur in the same beam and the sky position varies. Such events could occur from distant lightning, but we are currently unable to confirm that conjecture. The other clusters are similar. The majority of the events are seen in a single beam, however, events in cluster seven have been detected in up to three adjacent beams.

We currently have no easy means to determine which of these 202 events are worthy of follow-up (noting that for a future survey, we would apply these methods in close to real-time, allowing for a much quicker response time). Instead, we have chosen two events for a more detailed analysis.

In Fig. 6, we show one example where a bright event is seen in three adjacent beams. In this Figure, we show the region around the event in all 13 beams of the multibeam receiver with the panels approximately representing the positions of the beams. The UMAP

analysis is based on individual images presented to the algorithm. It does not account for any differences in the time of an event during those images. This is shown here where the signal is first seen in Beam 9, then less than a second later in Beam 2 and then in Beam 8. By setting the arrival time of Beam 9 as 0 sec, the arrival times of Beam 2 and Beam 8 are determined to be 0.618 sec and 1.007 sec, respectively. Because of this time difference, it is clear that this particular event is not an astronomical signal of interest and is representative of a satellite moving across the beams.

One of our most interesting sources is shown in Fig. 7. In this figure, we see a broadband signal that lasts a few seconds. However, through the 60-second observation, it repeats. These particular set of observations correspond to a test sequence of the multibeam system, where each beam in turn was pointed to the pulsar, PSR J2048–1616. We note that this pulsar is bright and it is possible to detect single pulses from the pulsar (which have a dispersion measure of $11.46 \text{ cm}^{-3} \text{ pc}$ and a width of 12ms). However, the pulsar

is always in a different beam from the signal of interest here and our signal was detected in eight of the 60-second observations with the source being consistently located at right ascension 20:47:34.4 and declination $-16:42:03$ ⁴. Images of these events are provided online at <https://astroyx.github.io/anomaly/>.

We have applied a 15 arc-min cone search in the CSIRO data archive (Hobbs et al. 2011) for this sky position and identified 11 observation files after P269-2001JANT. We have searched these files by eye and have not identified any similar event. The origin of this source is therefore currently unknown. Within a 0.23 deg radius, GAIA has identified a total of four sources located within 100 pc from the Earth. Table 2 lists the properties of these stars. Two of them are also stored by SIMBAD and more information is offered. One source “Gaia DR3 6886022079566800768” is a high proper motion star. The other source “Gaia DR3 6886074198993703168” is a white dwarf candidate. In a study conducted by Hurley-Walker et al. (2023), a long-period radio transient was discovered, exhibiting activity over a span of three decades. While highly magnetic isolated white dwarfs are expected to possess similar characteristics, no direct detection of periodic coherent radio emission has been found from these sources yet. We speculate that the observed anomaly could potentially be a stellar flare originating from one of the stars within the covered region. If the anomalous event comes from a white dwarf, then it could be the second confirmed radio active pulsar emitting white dwarf after AR Sco. We are requesting longer-term follow-up observations of the sky region to search for further events.

4 CONCLUSION

The UMAP unsupervised machine learning pipeline has the potential to identify anomalous signals in high-time-resolution data sets. Applying this pipeline to the P269-2001JANT dataset, we rediscovered the Lorimer burst from the dataset (Lorimer et al. 2007) and also identified a relatively large number of other events. A table containing the properties of these events is provided in the Appendix. The majority of these events have durations on a timescale of seconds, which corresponds to several solar radii. We note that because these observations were taken over two decades ago it may be impossible to identify the cause of many of these signals and hence this method has primarily been designed for the next generation of surveys carried out with the Murriyang Parkes radio telescope. Burke-Spolaor et al. (2011) found radio bursts with similar spectra to FRBs, but they were confirmed as terrestrial origins because of 13 beams simultaneously detection. The multibeam information is crucial for identifying signals originating from the universe.

A cryogenic phased array receiver (cryoPAF) is currently being completed and will be installed on the telescope in 2024. This receiver will increase the number of beams from 13 to 72 and the bit depth of the backend instrument will increase from the 1-bit data used in this paper to 2-bits or 8-bits per sample. Both of these improvements will enhance the UMAP algorithm. The higher bit precision will allow the features in the data streams to be better characterised. The large number of beams and more flexible backend system of the cryoPAF will allow us to develop new algorithms to mitigate RFI (Lourenco & Chippendale 2024), and we plan to develop the UMAP pipeline to explicitly incorporate the spatial information of the multiple beam signals.

⁴ The multibeam system covered the position for eight times with different beams, the standard deviation of the eight times of pointing for RA is 0.6 arc-sec, and 9.0 arc-sec for DEC. The sky coverage of each beam is ~ 0.23 deg.

The data processed here were all available in a single archive. This method of processing data will remain viable assuming that the raw data sets are archived. However, the increasing data volumes from radio telescopes often means that searches for transient events are carried out in real-time and only data surrounding events of interest are stored. Our pipeline can easily be converted into a “real-time” mode. An almost identical data set for clustering would occur if instead of picking 2,051 subintegrations from each of the three data files, we instead select 100 subintegrations from 72 input files. This would require a larger memory capacity, IO speed and parallel computing accelerator like A100 to accommodate this real-time processing.

ACKNOWLEDGEMENTS

This paper includes archived data obtained through the Parkes Pulsar Data Archive on the CSIRO Data Access Portal (<https://data.csiro.au/>). The computing resource is offered by Scientific Computing’s shared system in CSIRO. This work is partially supported by the National SKA Program of China (2022SKA0130100, 2020SKA0120300), the National Natural Science Foundation of China (grant Nos. 12041306, 12273113, 12233002, 12003028, 12321003), the CAS Project for Young Scientists in Basic Research (Grant No. YSBR-063), the International Partnership Program of Chinese Academy of Sciences for Grand Challenges (114332KYSB20210018), the National Key R&D Program of China (2021YFA0718500), the ACAMAR Postdoctoral Fellow, China Postdoctoral Science Foundation (grant No. 2020M681758), and the Natural Science Foundation of Jiangsu Province (grant Nos. BK20210998).

DATA AVAILABILITY STATEMENTS

The data used in this work is available from <https://data.csiro.au/>. Anomaly figures are available from <https://astroyx.github.io/anomaly/>.

REFERENCES

- Abdi H., Williams L. J., 2010, *WIREs Computational Statistics*, 2, 433
 Burke-Spolaor S., Bailes M., Ekers R., Macquart J.-P., Crawford Fronefield I., 2011, *ApJ*, 727, 18
 Crawford F., Kaspi V. M., Manchester R. N., Lyne A. G., Camilo F., D’Amico N., 2001, *ApJ*, 553, 367
 Dumas S., 2007, The 1999 and 2003 messages explained
 Giles D., Walkowicz L., 2019, *MNRAS*, 484, 834
 Gupta N., Huynh M., Norris R. P., Wang X. R., Hopkins A. M., Andernach H., Koribalski B. S., Galvin T. J., 2022, *Publ. Astron. Soc. Australia*, 39, e051
 Hobbs G., et al., 2011, *Publ. Astron. Soc. Australia*, 28, 202
 Hurley-Walker N., et al., 2022, *Nature*, 601, 526
 Hurley-Walker N., et al., 2023, *Nature*, 619, 487
 Lorimer D., Bailes M., McLaughlin M., Narkevic D., Crawford F., 2007, *Science*, 318, 777
 Lourenco L., Chippendale A. P., 2024, *arXiv e-prints*, p. arXiv:2405.16309
 Luo R., et al., 2022, *MNRAS*, 513, 5881
 Ma P. X., et al., 2023, *Nature Astronomy*, 7, 492
 Manchester R. N., Fan G., Lyne A. G., Kaspi V. M., Crawford F., 2006, *ApJ*, 649, 235
 Marianer T., Poznanski D., Prochaska J. X., 2021, *MNRAS*, 500, 5408
 McInnes L., Healy J., Melville J., 2018, *arXiv e-prints*, p. arXiv:1802.03426
 Norris R. P., 2017, *Publ. Astron. Soc. Australia*, 34, e007

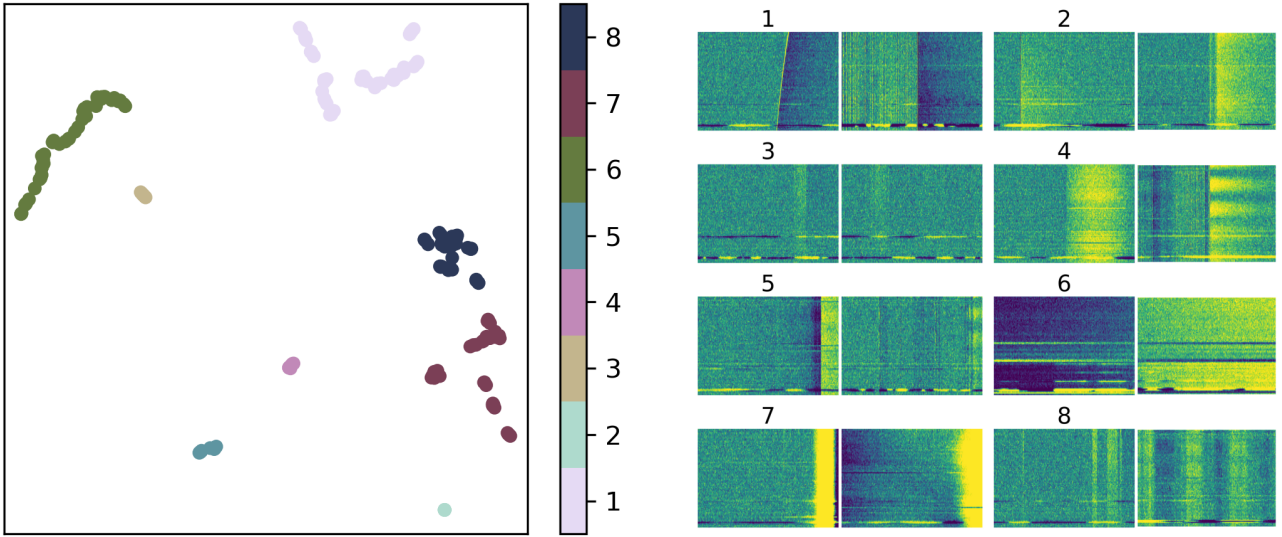


Figure 5. The left-hand panel shows the UMAP embedding of 202 anomalous events and Lorimer burst, the clusters are marked with different colours named from one to eight. The right-hand panel shows two representative figures of each cluster.

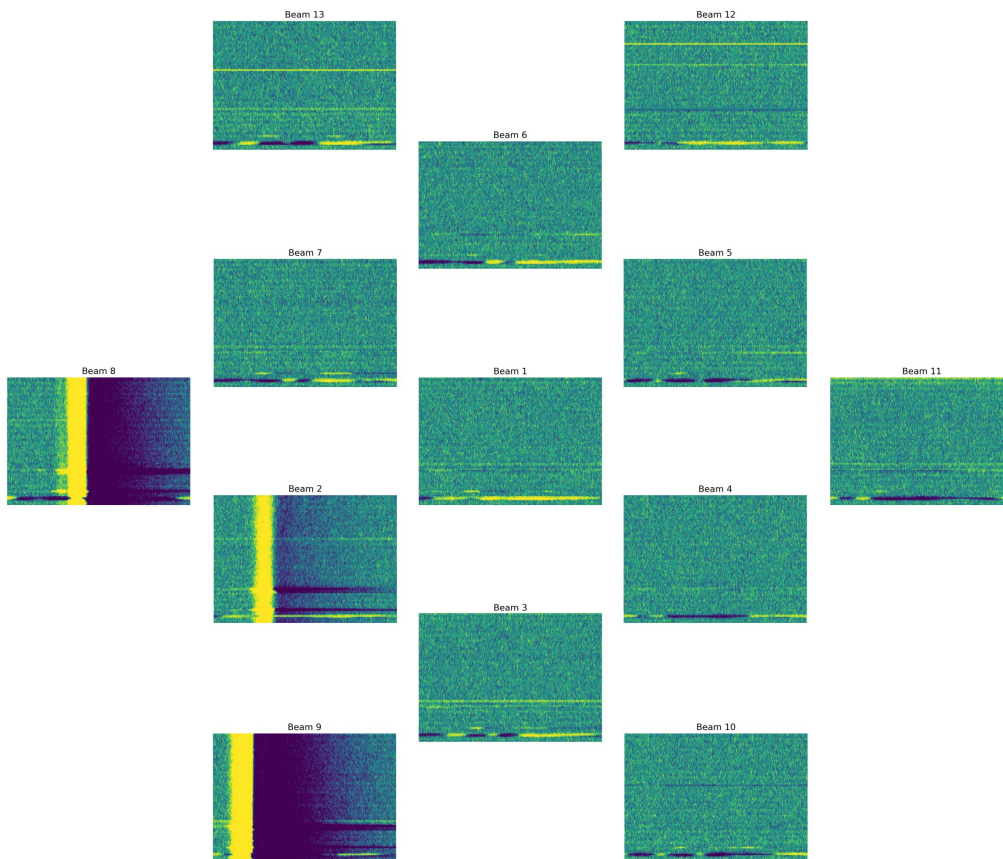


Figure 6. One of the anomalies from SMC019_01521, starts at time sample 5758976, and ends at 5763072. Each figure represents a time span of 4.096 seconds along the x-axis, 1,516.5 to 1,231.5 MHz from bottom to top along the y-axis.

Table 2. The sky position and parallax of four stars covered by the beam simultaneously.

Designation	RA	DEC	Parallax (mas)	Distance (pc)	Separation (deg)
Gaia DR3 6886022079566800768	20:48:13.15	-16:44:20.99	12.45	80.31	0.16
Gaia DR3 6886025824778303744	20:47:42.68	-16:42:45.75	10.73	93.15	0.04
Gaia DR3 6886074198993703168	20:47:19.19	-16:38:20.56	11.59	86.31	0.09
Gaia DR3 6886079322892555136	20:47:18.86	-16:29:43.01	17.58	56.90	0.21

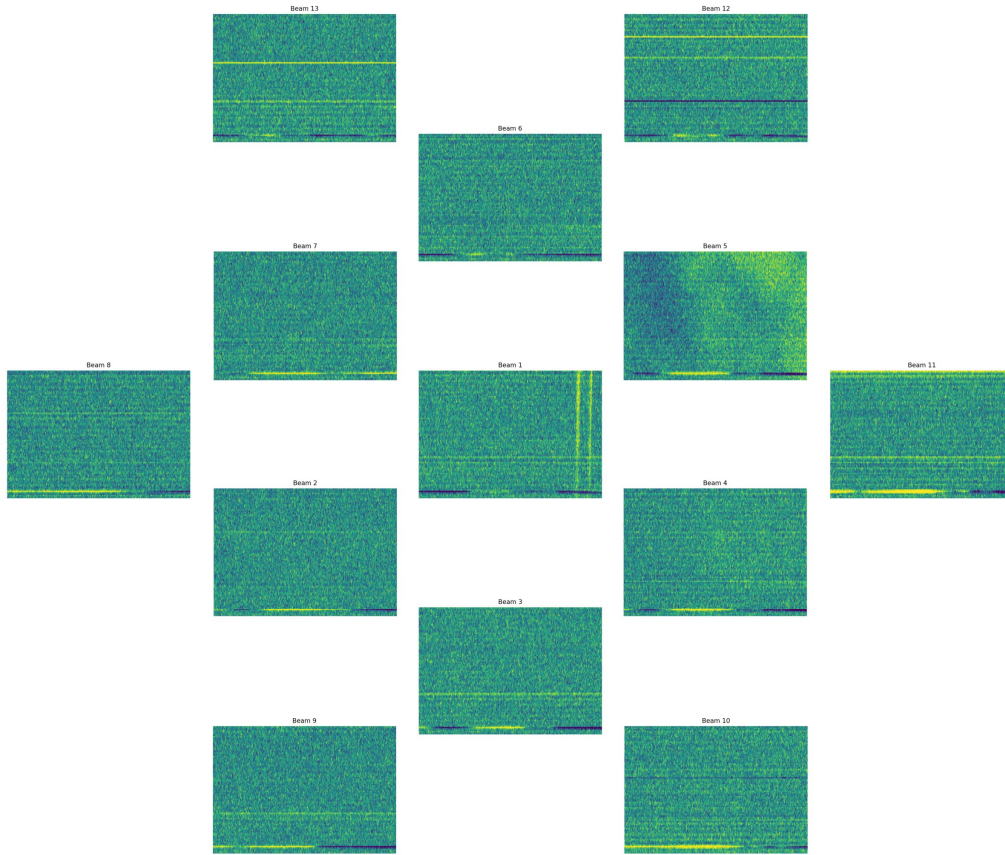


Figure 7. One of the anomalies from SMC017_02351.sf, starts at time sample 159744, and ends at 163840. The beam 1 was pointing at PSR J2048–1616. The anomaly detected by UMAP is in beam 5, and the other figures are the multibeam receiver’s observation simultaneously. Each figure represents 1.024 seconds of observation along the x-axis, 1,516.5 to 1,231.5 MHz from bottom to top along the y-axis. The GIF version of the one-minute multibeam observation can be found at <https://astroyx.github.io/anomaly/>, GIF column.

Ransom S., 2011, PRESTO: Pulsar Exploration and Search TOolkit (ascl:1107.017)

Ravi V., et al., 2016, *Science*, 354, 1249

Sheikh S. Z., et al., 2021a, *Nature Astronomy*, 5, 1153

Sheikh S. Z., et al., 2021b, *Nature Astronomy*, 5, 1153

Thornton D., et al., 2013, *Science*, 341, 53

Van der Maaten L., Hinton G., 2008, *Journal of machine learning research*, 9

Webb S., et al., 2020, *MNRAS*, 498, 3077

Wilkinson P. N., Kellermann K. I., Ekers R. D., Cordes J. M., W. Lazio T. J., 2004, *New Astron. Rev.*, 48, 1551

Yang X., Zhang S. B., Wang J. S., Wu X. F., 2023, *MNRAS*, 522, 4342

Yong S. Y., et al., 2022, *MNRAS*, 516, 5832

Zhang S. B., Hobbs G., Dai S., Toomey L., Staveley-Smith L., Russell C. J., Wu X. F., 2019, *MNRAS*, 484, L147

Zhang S. B., et al., 2020, *ApJS*, 249, 14

APPENDIX

This paper has been typeset from a \TeX/L\TeX file prepared by the author.

Table 3. The properties of anomalous events detected in this work. This table is slightly different from the one in Github since all the continuous observations are merged into one line.

Filename	RA	Dec	Galactic longitude	Galactic latitude	Time sample start	Time sample end	Duration(s)	MJD
SMC017_00621	05:18:25.51	-66:35:54.53	276.8443	-33.9195	1048576	1052672	4.096	51943.2069626852
SMC017_00621	05:18:25.51	-66:35:54.53	276.8443	-33.9195	1519616	1523712	4.096	51943.2124145370
SMC017_00811	05:20:46.00	-66:10:26.97	276.2943	-33.7574	3731456	3735552	4.096	51943.3705261111
SMC017_00821	05:15:57.96	-66:10:51.13	276.3992	-34.2343	102400	106496	4.096	51943.3285231481
SMC017_00821	05:15:57.96	-66:10:51.13	276.3992	-34.2343	1675264	1679360	4.096	51943.3467275926
SMC017_02351	20:47:34.66	-16:41:54.83	29.9414	-33.0079	0	262144	65.536	51944.1695023148
SMC017_02411	20:47:34.93	-16:41:55.86	29.9416	-33.0090	0	262144	65.536	51944.1706134259
SMC017_02541	20:47:34.92	-16:41:56.95	29.9412	-33.0091	0	262144	65.536	51944.1717592593
SMC017_026B1	20:47:34.66	-16:42:18.30	29.9342	-33.0103	0	262144	65.536	51944.1728587963
SMC017_028C1	20:47:33.06	-16:42:3.79	29.9358	-33.0029	0	262144	65.536	51944.1750925926
SMC017_02961	20:47:34.41	-16:41:53.82	29.9413	-33.0069	0	262144	65.536	51944.1762152778
SMC017_03071	20:47:34.65	-16:42:17.19	29.9345	-33.0102	0	262144	65.536	51944.1773263889
SMC017_03131	20:47:34.11	-16:42:9.15	29.9360	-33.0073	0	262144	65.536	51944.1785532407
SMC017_036D1	05:30:28.92	-68:48:6.43	279.2278	-32.4428	24576	28672	4.096	51944.1996478704
SMC017_037A1	05:28:03.97	-62:27:57.26	271.7613	-33.4167	2895872	2899968	4.096	51944.3306582407
SMC017_03991	05:18:17.54	-67:22:21.90	277.7651	-33.7968	3289088	3293184	4.096	51947.3206144444
SMC017_03991	05:18:17.54	-67:22:21.90	277.7651	-33.7968	3948544	3952640	4.096	51947.3282470370
SMC017_04041	05:36:03.33	-69:07:1.19	279.5171	-31.9046	2363392	2367488	4.096	51948.3073193519
SMC017_04041	05:36:03.33	-69:07:1.19	279.5171	-31.9046	2555904	2560000	4.096	51948.3095475000
SMC017_04041	05:36:03.33	-69:07:1.19	279.5171	-31.9046	2723840	2727936	4.096	51948.3114912037
SMC017_04041	05:36:03.33	-69:07:1.19	279.5171	-31.9046	2891776	2895872	4.096	51948.3134349074
SMC017_04041	05:36:03.33	-69:07:1.19	279.5171	-31.9046	3035136	3039232	4.096	51948.3150941667
SMC017_040A1	05:32:59.66	-68:42:41.20	279.0845	-32.2300	4390912	4395008	4.096	51948.3307860185
SMC017_04221	05:31:47.07	-68:56:37.37	279.3743	-32.3064	8269824	8273920	4.096	51952.4801021296
SMC017_04221	05:31:47.07	-68:56:37.37	279.3743	-32.3064	8294400	8298496	4.096	51952.4803865741
SMC017_04231	05:37:09.63	-68:54:19.80	279.2558	-31.8321	5672960	5677056	4.096	51952.4500458333
SMC017_04341	05:37:41.74	-69:19:21.74	279.7364	-31.7350	110592	114688	4.096	51952.4832244444
SMC017_04341	05:37:41.74	-69:19:21.74	279.7364	-31.7350	1118208	1122304	4.096	51952.4948866667
SMC017_04341	05:37:41.74	-69:19:21.74	279.7364	-31.7350	1286144	1290240	4.096	51952.4968303704
SMC017_04341	05:37:41.74	-69:19:21.74	279.7364	-31.7350	1642496	1646592	4.096	51952.5009548148
SMC017_04341	05:37:41.74	-69:19:21.74	279.7364	-31.7350	1662976	1667072	4.096	51952.5011918519
SMC017_04341	05:37:41.74	-69:19:21.74	279.7364	-31.7350	2019328	2023424	4.096	51952.5053162963
SMC017_04341	05:37:41.74	-69:19:21.74	279.7364	-31.7350	2125824	2129920	4.096	51952.5065488889
SMC017_043C1	05:32:54.81	-70:12:20.46	280.8324	-32.0256	3182592	3186688	4.096	51952.5187800000
SMC017_07531	05:45:32.45	-72:17:10.16	283.0872	-30.7409	5218304	5226496	8.192	51956.3316238889
SMC017_07531	05:45:32.45	-72:17:10.16	283.0872	-30.7409	5230592	5234688	4.096	51956.3317661111
SMC017_07531	05:45:32.45	-72:17:10.16	283.0872	-30.7409	5246976	5251072	4.096	51956.3319557407
SMC017_07541	05:51:50.61	-72:13:12.21	282.9525	-30.2702	5259264	5267456	8.192	51956.3320979630
SMC017_07541	05:51:50.61	-72:13:12.21	282.9525	-30.2702	5283840	5287936	4.096	51956.3323824074
SMC017_07541	05:51:50.61	-72:13:12.21	282.9525	-30.2702	5292032	5296128	4.096	51956.3324722022
SMC018_00781	05:43:55.68	-69:26:57.40	279.8144	-31.1760	2629632	2637824	8.192	51971.3200420370
SMC018_02451	05:41:29.34	-67:04:10.39	277.0607	-31.6109	5685248	5689344	4.096	51977.3814380556
SMC018_02451	05:41:29.34	-67:04:10.39	277.0607	-31.6109	5693440	5701632	8.192	51977.3815328704
SMC018_02451	05:41:29.34	-67:04:10.39	277.0607	-31.6109	5738496	5746688	8.192	51977.3820543519
SMC018_02451	05:41:29.34	-67:04:10.39	277.0607	-31.6109	5869568	5873664	4.096	51977.3835713889
SMC018_02451	05:41:29.34	-67:04:10.39	277.0607	-31.6109	5885952	5890048	4.096	51977.3837610185
SMC018_02451	05:41:29.34	-67:04:10.39	277.0607	-31.6109	5902336	5906432	4.096	51977.3839506481
SMC018_02451	05:41:29.34	-67:04:10.39	277.0607	-31.6109	5947392	5951488	4.096	51977.3844721296
SMC018_02451	05:41:29.34	-67:04:10.39	277.0607	-31.6109	6000640	6004736	4.096	51977.3850884259
SMC018_02451	05:41:29.34	-67:04:10.39	277.0607	-31.6109	6029312	6033408	4.096	51977.3854202778
SMC018_02451	05:41:29.34	-67:04:10.39	277.0607	-31.6109	6549504	6553600	4.096	51977.3914410185
SMC018_02451	05:41:29.34	-67:04:10.39	277.0607	-31.6109	6561792	6565888	4.096	51977.3915832407
SMC018_02451	05:41:29.34	-67:04:10.39	277.0607	-31.6109	6594560	6602752	8.192	51977.3919625000
SMC018_02451	05:41:29.34	-67:04:10.39	277.0607	-31.6109	6639616	6643712	4.096	51977.3924839815
SMC018_02451	05:41:29.34	-67:04:10.39	277.0607	-31.6109	6676480	6680576	4.096	51977.3929106481
SMC018_02451	05:41:29.34	-67:04:10.39	277.0607	-31.6109	6742016	6746112	4.096	51977.3936691667
SMC018_02451	05:41:29.34	-67:04:10.39	277.0607	-31.6109	6770688	6774784	4.096	51977.3940010185
SMC018_02451	05:41:29.34	-67:04:10.39	277.0607	-31.6109	6787072	6791168	4.096	51977.3941906481
SMC018_02451	05:41:29.34	-67:04:10.39	277.0607	-31.6109	6807552	6811744	8.192	51977.3944276852
SMC018_02451	05:41:29.34	-67:04:10.39	277.0607	-31.6109	6819840	6823936	4.096	51977.3945699074
SMC018_02451	05:41:29.34	-67:04:10.39	277.0607	-31.6109	6828032	6832128	4.096	51977.3946647222
SMC018_02451	05:41:29.34	-67:04:10.39	277.0607	-31.6109	6844416	6848512	4.096	51977.3948543518
SMC018_02451	05:41:29.34	-67:04:10.39	277.0607	-31.6109	7102464	7122944	20.480	51977.3978410185
SMC018_02451	05:41:29.34	-67:04:10.39	277.0607	-31.6109	7143424	7151616	8.192	51977.3983150926
SMC018_02451	05:41:29.34	-67:04:10.39	277.0607	-31.6109	7462912	7467008	4.096	51977.4020128704
SMC018_02451	05:41:29.34	-67:04:10.39	277.0607	-31.6109	7471104	7475200	4.096	51977.4021076852
SMC018_02451	05:41:29.34	-67:04:10.39	277.0607	-31.6109	7495680	7507968	12.288	51977.4023921296
SMC018_02451	05:41:29.34	-67:04:10.39	277.0607	-31.6109	7512064	7516160	4.096	51977.4025817593
SMC018_02451	05:41:29.34	-67:04:10.39	277.0607	-31.6109	8007680	8011776	4.096	51977.4083180556
SMC018_02451	05:41:29.34	-67:04:10.39	277.0607	-31.6109	8015872	8019968	4.096	51977.4084128704
SMC018_02651	05:44:23.32	-66:24:36.67	276.2656	-31.3723	4894720	4898816	4.096	51978.2399620370
SMC018_02651	05:44:23.32	-66:24:36.67	276.2656	-31.3723	4902912	4907008	4.096	51978.2400568519
SMC018_02651	05:44:23.32	-66:24:36.67	276.2656	-31.3723	4984832	4993024	8.192	51978.2410050000
SMC018_02651	05:44:23.32	-66:24:36.67	276.2656	-31.3723	4997120	5005312	8.192	51978.2411472222
SMC018_02651	05:44:23.32	-66:24:36.67	276.2656	-31.3723	5033984	5038080	4.096	51978.2415738889
SMC018_02651	05:44:23.32	-66:24:36.67	276.2656	-31.3723	5062656	5066752	4.096	51978.2419057407
SMC019_001D1	05:38:18.98	-64:15:45.57	273.7916	-32.1388	12288	16384	4.096	51982.2663459259

Table 3. Continued.

Filename	RA	Dec	Galactic longitude	Galactic latitude	Time sample start	Time sample end	Duration(s)	MJD
SMC019_00241	05:47:36.20	-63:30:57.29	272.8665	-31.1483	1646592	1650688	4.096	51982.3828077778
SMC019_01521	05:20:53.78	-72:26:25.98	283.6415	-32.5527	5758976	5763072	4.096	52039.0119210185
SMC019_01811	05:52:32.00	-72:38:13.02	283.4275	-30.1801	1011712	1015808	4.096	52040.1888739815
SMC019_01811	05:52:32.00	-72:38:13.02	283.4275	-30.1801	1167360	1175552	8.192	52040.1906754630
SMC019_01811	05:52:32.00	-72:38:13.02	283.4275	-30.1801	1179648	1183744	4.096	52040.1908176852
SMC019_01811	05:52:32.00	-72:38:13.02	283.4275	-30.1801	1208320	1212416	4.096	52040.1911495370
SMC019_01811	05:52:32.00	-72:38:13.02	283.4275	-30.1801	1249280	1253376	4.096	52040.1916236111
SMC019_01811	05:52:32.00	-72:38:13.02	283.4275	-30.1801	1261568	1265664	4.096	52040.1917658333
SMC019_01811	05:52:32.00	-72:38:13.02	283.4275	-30.1801	1269760	1277952	8.192	52040.1918606481
SMC019_01811	05:52:32.00	-72:38:13.02	283.4275	-30.1801	1306624	1310720	4.096	52040.1922873148
SMC019_01811	05:52:32.00	-72:38:13.02	283.4275	-30.1801	3727360	3731456	4.096	52040.2203050926
SMC019_01811	05:52:32.00	-72:38:13.02	283.4275	-30.1801	3735552	3756032	20.480	52040.2203999074
SMC019_01811	05:52:32.00	-72:38:13.02	283.4275	-30.1801	3764224	3768320	4.096	52040.2207317593
SMC019_01811	05:52:32.00	-72:38:13.02	283.4275	-30.1801	3878912	3887104	8.192	52040.2220591667
SMC019_01811	05:52:32.00	-72:38:13.02	283.4275	-30.1801	3891200	3895296	4.096	52040.2222013889
SMC019_01811	05:52:32.00	-72:38:13.02	283.4275	-30.1801	3985408	3993600	8.192	52040.2232917593
SMC019_01811	05:52:32.00	-72:38:13.02	283.4275	-30.1801	4009984	4014080	4.096	52040.2235762037
SMC019_01811	05:52:32.00	-72:38:13.02	283.4275	-30.1801	4018176	4022272	4.096	52040.2236710185
SMC019_01811	05:52:32.00	-72:38:13.02	283.4275	-30.1801	4046848	4055040	8.192	52040.2240028704
SMC019_01811	05:52:32.00	-72:38:13.02	283.4275	-30.1801	4059136	4063232	4.096	52040.2241450926
SMC019_01811	05:52:32.00	-72:38:13.02	283.4275	-30.1801	4087808	4096000	8.192	52040.2244769444
SMC019_01951	05:49:26.41	-68:24:3.98	278.5503	-30.7647	6905856	6909952	4.096	52040.3549636111
SMC019_01951	05:49:26.41	-68:24:3.98	278.5503	-30.7647	6914048	6918144	4.096	52040.3550584259
SMC019_01951	05:49:26.41	-68:24:3.98	278.5503	-30.7647	6922240	6930432	8.192	52040.3551532407
SMC019_01951	05:49:26.41	-68:24:3.98	278.5503	-30.7647	6942720	6959104	16.384	52040.3553902778
SMC019_01951	05:49:26.41	-68:24:3.98	278.5503	-30.7647	6963200	6967296	4.096	52040.3556273148
SMC019_01951	05:49:26.41	-68:24:3.98	278.5503	-30.7647	7213056	7217152	4.096	52040.3585191667
SMC019_01951	05:49:26.41	-68:24:3.98	278.5503	-30.7647	7241728	7245824	4.096	52040.3588510185
SMC019_01951	05:49:26.41	-68:24:3.98	278.5503	-30.7647	7258112	7262208	4.096	52040.3590406482
SMC019_01951	05:49:26.41	-68:24:3.98	278.5503	-30.7647	7278592	7282688	4.096	52040.3592776852
SMC019_02051	05:57:25.53	-69:55:35.53	280.2717	-29.9742	7663616	7671808	8.192	52041.3221182407
SMC019_02051	05:57:25.53	-69:55:35.53	280.2717	-29.9742	7708672	7712768	4.096	52041.3221639722
SMC019_02051	05:57:25.53	-69:55:35.53	280.2717	-29.9742	7766016	7770112	4.096	52041.3223034259
SMC019_02051	05:57:25.53	-69:55:35.53	280.2717	-29.9742	7778304	7782400	4.096	52041.3224456481
SMC019_02611	05:41:13.01	-63:36:4.02	272.9925	-31.8562	4734976	4739072	4.096	52068.2370020370
SMC019_02611	05:41:13.01	-63:36:4.02	272.9925	-31.8562	5136384	5140480	4.096	52068.2416479630
SMC019_02611	05:41:13.01	-63:36:4.02	272.9925	-31.8562	5144576	5148672	4.096	52068.2417427778
SMC019_02611	05:41:13.01	-63:36:4.02	272.9925	-31.8562	5160960	5165056	4.096	52068.2419324074
SMC019_02611	05:41:13.01	-63:36:4.02	272.9925	-31.8562	5169152	5173248	4.096	52068.2420272222
SMC019_02611	05:41:13.01	-63:36:4.02	272.9925	-31.8562	5210112	5214208	4.096	52068.2425012963
SMC019_02611	05:41:13.01	-63:36:4.02	272.9925	-31.8562	5222400	5226496	4.096	52068.2426435185
SMC019_02611	05:41:13.01	-63:36:4.02	272.9925	-31.8562	5439488	5443584	4.096	52068.2451561111
SMC019_02611	05:41:13.01	-63:36:4.02	272.9925	-31.8562	7901184	7905280	4.096	52068.2736479630
SMC019_04011	00:13:05.00	-74:56:12.07	306.2684	-41.9422	237568	241664	4.096	52068.9535713889
SMC019_04011	00:13:05.00	-74:56:12.07	306.2684	-41.9422	249856	253952	4.096	52068.9537136111
SMC019_04011	00:13:05.00	-74:56:12.07	306.2684	-41.9422	282624	286720	4.096	52068.9540928704
SMC019_04011	00:13:05.00	-74:56:12.07	306.2684	-41.9422	315392	319488	4.096	52068.9544721296
SMC019_04011	00:13:05.00	-74:56:12.07	306.2684	-41.9422	323584	327680	4.096	52068.9545669444
SMC019_04311	00:11:56.00	-74:42:56.92	306.4279	-42.1432	4886528	4890624	4.096	52070.0717075000
SMC020_002A1	05:56:59.73	-65:25:30.57	275.0735	-30.1178	6930432	6934528	4.096	52073.3105258333
SMC020_00421	00:36:29.50	-74:56:26.50	304.2406	-42.1496	1060864	1064960	4.096	52074.9106234259
SMC020_00421	00:36:29.50	-74:56:26.50	304.2406	-42.1496	1081344	1085440	4.096	52074.9108604630
SMC020_00421	00:36:29.50	-74:56:26.50	304.2406	-42.1496	1097728	1101824	4.096	52074.9110500926
SMC020_00421	00:36:29.50	-74:56:26.50	304.2406	-42.1496	1105920	1110016	4.096	52074.9111449074
SMC020_00421	00:36:29.50	-74:56:26.50	304.2406	-42.1496	1126400	1130496	4.096	52074.9113819444
SMC020_00421	00:36:29.50	-74:56:26.50	304.2406	-42.1496	3092480	3104768	12.288	52074.9341375000
SMC020_00421	00:36:29.50	-74:56:26.50	304.2406	-42.1496	3149824	3153920	4.096	52074.9348012037
SMC020_00451	00:43:02.00	-75:49:5.34	303.6170	-41.2989	8396800	8400896	4.096	52074.9955300926
SMC020_00521	00:32:55.05	-74:54:57.66	304.5557	-42.1538	4452352	4456448	4.096	52078.9452008333
SMC020_00521	00:32:55.05	-74:54:57.66	304.5557	-42.1538	4464640	4468736	4.096	52078.9453430556
SMC020_00621	01:17:09.75	-74:22:4.11	300.5804	-42.6428	1806336	1810432	4.096	52079.9058719444
SMC020_00621	01:17:09.75	-74:22:4.11	300.5804	-42.6428	2621440	2625536	4.096	52079.9153060185
SMC020_00621	01:17:09.75	-74:22:4.11	300.5804	-42.6428	3043328	3047424	4.096	52079.9201889815
SMC021_00221	01:17:28.88	-74:47:14.37	300.6292	-42.2243	7708672	7712768	4.096	52080.8708526852
SMC021_00281	01:14:05.15	-75:13:32.08	300.9973	-41.8175	4640768	4644864	4.096	52080.8353445370
SMC021_002D1	01:26:14.27	-75:35:8.97	300.0570	-41.3476	651264	655360	4.096	52080.7891697222
SMC021_00321	01:18:39.82	-74:09:27.28	300.4031	-42.8367	6295552	6299648	4.096	52081.9552378704
SMC022_00121	04:21:33.61	-70:58:53.67	283.9290	-37.4108	7712768	7716864	4.096	52146.6826362037